Laser diode array side-pumped medium-aperture Nd:glass square rod amplifier

Xiongxin Tang (唐熊忻), Jisi Qiu (邱基斯)*, Zhongwei Fan (樊仲维), Haocheng Wang (王昊成), and Weiran Lin (林蔚然)**

The Academy of Opto-Electronics, Chinese Academy of Sciences, Beijing 10094, China
**Corresponding author: keith0311@163.com; **corresponding author: fanzhongwei@aoe.ac.cn*
Received September 17, 2015; accepted November 19, 2015; posted online January 26, 2016

A laser diode array side-pumped Nd:glass square rod amplifier of the dimensions 12 mm × 12 mm is designed. The fluorescence is evenly distributed in the Nd:glass amplifier. When the pump power is 66.32 kW, the small signal gain increases by 3.23 times. Under the condition of a 1 Hz repetition frequency, 50 mJ of injected seed-light energy, and a 10 mm × 10 mm aperture, the output energy of the laser beam can reach 1.62 J during the four-pass amplification. The output energy stability of the laser pulse is 2.94% (RMS), and the square pulse distortion is smaller than 2. The energy amplification of the injected laser beam from millijoules to joules is realized.

OCIS codes: 140.3480, 140.5560, 140.2010, 140.0140.
doi: 10.3788/COL201614.021403.

Nd:glass has good optical homogeneity, a high doping concentration, a suitable stimulated emission cross section, and a big gain bandwidth (more than 20 nm). Thus, it becomes the best medium for the inertial confinement fusion (ICF) laser drive in the study of high-power drivers[1–5]. Currently, flash lamp pumping is often adopted for a medium-aperture beam energy amplification where Nd:glass is the working medium[6,7]. But a big amount of energy will get lost in the form of heat, since the too-wide spectrum launched by a xenon lamp will not be well matched with the Nd:glass absorption spectrum. Additionally, a severe heat effect will be caused under the condition of a huge amount of energy due to the low heat transfer coefficient (N31, for example: 5.58 W/(cm°C)), which will take really a long time to cool off and eliminate the thermal distortion. Therefore, it is quite difficult to achieve a repetitive operation. But repetitive frequency operation is the development trend for high-power laser drivers[8]. Both the repetitive frequency operation and the laser of the energy output up from joules to thousands of joules are the keys for promoting the laser-matter interaction and the study and development of inertial fusion energy, which also enjoys promising application prospects in the industrial and medical fields.

Diode-array-pumped solid-state lasers have many advantages, like high light-conversion efficiency, a long working life, good beam quality and high reliability, etc. Laser diode array pumping has developed rapidly since 1990s, and has been widely adopted by the new generation of solid-state lasers[9–11]. Actually, certain achievements have been made in the aspect of laser diode-pumped Nd:glass. For example, Deng *et al.*[12] further developed the laser diode-pumped small-aperture (Φ2 mm) Nd:glass round rod amplifier. When the pump power reached 7.7 kW, the small signal gain increased by 40 times. Zhao *et al.*[13] designed a multi-pass traveling wave amplifier based on an end-pumping Nd:glass slice used to amplify 8 mm × 8 mm signal lasers from 300 μJ to 246 mJ. However, there have been few reports on the study of laser diode array side-pumped medium-aperture Nd:glass amplifiers.

In the research and development of laser drivers for ICF, the beam shape is designed as a square in order to facilitate the fill factor and energy extraction efficiency of the slab amplifier[14–16]. Thus, higher energy extraction efficiency could be achieved if the working medium for the preamplifier was a square. Therefore, in this research, an aperture 12 mm × 12 mm Nd:glass square rod amplifier with a laser diode array pump is developed. When the pump power reaches 66.32 kW, the small signal gain increases by 3.23 times. In addition, the designed four-pass amplifying light path realizes the amplification of the output beam to the level of joules from the input level of millijoules. The output energy stability of the laser pulse is 2.94% (RMS), and the square pulse distortion is smaller than 2.

For the rectangular pulse, the gain could be expressed as

$$G = \frac{E_s}{E_{\text{in}}} \ln\left\{1 + \left[\exp\left(\frac{E_{\text{in}}}{E_s}\right) - 1\right] G_0\right\}, \tag{1}$$

where E_{in} is the injected pulse-energy density, E_s is the saturated energy density, and $G_0 = \exp(g_0 l)$ is the small signal one-way gain. The saturated energy density is defined as

$$E_s = \frac{h\nu}{\gamma\sigma}. \tag{2}$$

In the four-level system, $\gamma = 1$[17], and the stimulated radiation cross-section area of N31 Nd:glass $\sigma = 3.8 \times 10^{-20}$ cm^2[18], then the saturated energy density can be calculated. When $E_{\text{in}}/E_s \ll 1$, G could be approximated as

 © 2016 Chinese Optics Letters

$$G \approx G_0 = \exp(g_0 l) = \exp\left(\frac{E_{\rm st}\sigma l}{h\nu}\right) = \exp\left(\frac{E_{\rm st} A l}{E_s A}\right) = \exp\left(\frac{\varepsilon_{\rm st}}{E_s A}\right), \quad (3)$$

where $g_0 = n\sigma$, energy storage density $E_{\rm st} = nh\nu$, and A and l are the cross-section area and length of the gain medium of the light region. The effective gain medium energy storage is $\varepsilon_{\rm st} = E_{\rm st} Al$.

Connected with the energy transport mechanism, the small signal gain could be expressed as

$$G_0 = \exp\left(\frac{\eta_{\rm st}\eta_s\eta_q\eta_{a-{\rm eff}}\eta_t P_p t_p}{E_s A}\right), \quad (4)$$

where P_p is the pumping source peak power, and t_p is the pump pulse width. A transmission efficiency of $\eta_t = 90\%$ is the empirical estimation of the side-pumped structure. The effective absorption efficiency is $\eta_{a-{\rm eff}} = 54.4\%$. It is the 802 nm light absorption passing through the light region, which is the result of the gain medium absorption efficiency multiplied by the pattern-matching efficiency. A quantum efficiency of $\eta_q = 85\%$[17] is the Nd:glass material's property. A Stokes' efficiency of $\eta_s = 76.2\%$ is the ratio between the pumped light wavelength and the laser wavelength, 802/1053 nm.

The energy storage efficiency can be obtained as

$$\eta_{\rm st} = \frac{1 - \exp(-t_p/\tau_f)}{t_p/\tau_f}, \quad (5)$$

where $t_p = 440$ μs is the pulse width, $t_p = 340$ μs[19] is the Nd:glass fluorescence lifetime, and $\eta_{\rm st} = 56.1\%$.

With a laser rod of 12 mm × 12 mm × 160 mm, 66.32 kW of pump power, and with a 3.5 mm distance from the laser diode array's shiny surface to the laser rod's surface, the pumped light intensity distribution across the laser medium cross section is simulated as in Fig. 1, which illustrates that the pumped light intensity is evenly distributed. It is obtained from the calculation and modeling by Zemax optical design software.

During the multi-pass amplification, the pre-pass output energy is just the input energy for the next pass. Considering the loss of the amplifier, the laser output energy is

$$E_{n+1,{\rm in}} = TE_{n,{\rm out}}, \quad (6)$$

where the subscript n stands for the nth-pass amplification, T is the amplifier static one-way transmittance, which is estimated as 85%. ε is the energy storage; the energy extraction efficiency η_E is the quotient of the energy extracted from the amplifier divided by the upper-level laser stored energy while the pulse arrives at the amplifier, which could be expressed as

$$\eta_E = \frac{E_{\rm out} - E_{\rm in}}{\varepsilon_{\rm st}}. \quad (7)$$

In the process of the multi-pass amplification, the stored energy of each pass could be expressed as

$$\varepsilon_{n+1,{\rm st}} = \varepsilon_{n,{\rm st}} - (E_{n,{\rm out}} - E_{n,{\rm in}}) = (1 - \eta_{n,E})\varepsilon_{n,{\rm st}}. \quad (8)$$

When the input energy is 50 mJ under a pump power of 33.63 kW, the output energy of each pass is shown in Fig. 2. The rest of the stored energy and the energy extraction efficiency of each pass of the amplifier are shown in Fig. 3. The abscissa shows the times of the laser passing through the amplifier. From Fig. 3, it can be seen that the total stored energy of the amplifier is 5.63 J, and the stored energy after the fourth-pass amplification is 3.70 J. The output energy of the laser is up to 1.5 J (seen from Fig. 2), and thus the extraction efficiency is 34.32%. The stored energy out of the seventh-pass amplification is 0.72 J, and the extraction efficiency is 87.2%. At this point, the stored energy has almost been completely extracted.

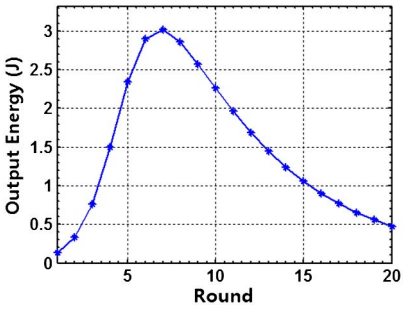

Fig. 2. Output energy of multi-pass amplification.

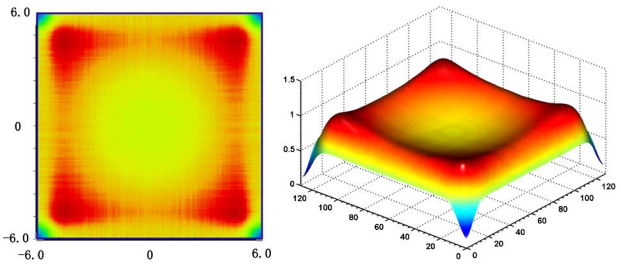

Fig. 1. Laser rod cross-section pumped-light two-dimensional and three-dimensional distribution map.

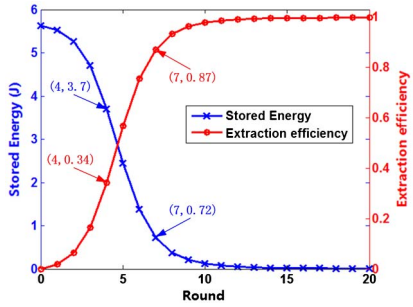

Fig. 3. Amplifier stored energy and energy extraction efficiency after multi-pass amplification.

Meanwhile, a simulation and calculation are done on the time waveform of a 5 ns square-wave seed pulse after the multi-pass amplification shown in Fig. 4. The square pulse distortion is defined as the ratio between the pulse front and back power, which is usually less than 2 in the design of the laser amplifier. Figure 4 shows that the time waveform distortion becomes bigger along with the increase of the pass, and the value is 1.51 after the fourth-pass amplification. Thus, to realize the amplification of the output beam energy to the level of joules from the input level of millijoules, four passes are designed for the amplification, considering the energy extraction efficiency and square pulse distortion.

The Nd:glass square rod amplifier structure is shown in Fig. 5. The laser diode vertical-stacked array pump is adopted (the bar is perpendicular to the Nd:glass rod). Each laser diode stacked array includes 60 bars, and the maximum output power for each bar is 300 W of the fast axis divergence angle 70° (FWHM) and the slow axis divergence angle 16° (90%E). The polarization mode of the pump light is TM. The laser diode stacked array parameters are as follows: 1.2 mm pitch distance, (W)10 mm × (L)70.8 mm emission region, less than 4 nm (FWHM) spectrum width, and 52% electro-optical efficiency. The deviation of the four-stack center wavelength is less than 1 nm, and the stability of these laser diodes is 0.5%. The N31 Nd:glass square rod of the size 12 mm × 12 mm × 160 mm with an effective pump length of 100 mm and a doping concentration of 1.2% is manufactured by the Shanghai Institute of Ceramics, the Chinese Academy of Sciences. A 2° dip angle is designed on both ends of the Nd:glass to avoid self-excited oscillation. A 1053 nm anti-reflection coating is plated on both ends of the rod to reduce loss. In the experiment, the central wavelength of the laser diode array is 802 nm. The macro-channel water-cooling structure is adopted for cooling off the laser diode array, and the temperature is controlled at 20°C.

A fluorescence spectrometer is used for testing the fluorescence distribution of Nd:glass amplifier as shown in Fig. 6, from which it can be seen that the pumped light intensity in the Nd:glass square rod amplifier is evenly distributed. The tested distribution form of the pumped light intensity is coincident with the simulation result shown in Fig. 1.

A pulse light source with a repetition frequency of 1 Hz, a wavelength of 1053 nm, a pulse width of 5 ns, an energy of 50 mJ, and a beam aperture of 10 mm × 10 mm is taken as the small-signal seed light for testing the small signal gain of the Nd:glass amplifier. When the laser diode water cools off to 20°C and the pump pulse width is 440 μs, the pump power is between 15.12 and 66.32 kW, and the output energy is recorded with the interval of 5.12 kW. The energy meter is placed 2.3 m behind the amplifier to avoid the influence of spontaneous radiation and the pumped light. Figure 7 provides the measured and theoretical calculated diagrams between the pump power and the gain ratio, from which a good agreement can be seen between the actual experiment result and the theoretical calculation. When the pump power is 66.32 kW, the Nd:glass amplifier increases by 3.23 times.

In order to realize the amplification of the output beam to the level of joules from the input level of millijoules, a

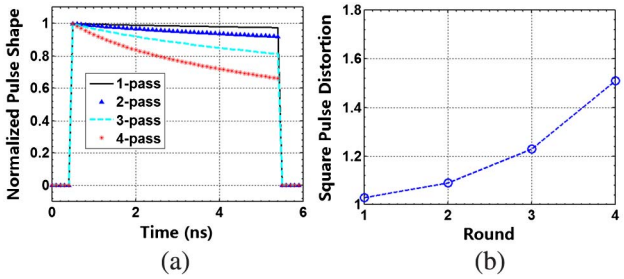

Fig. 4. (a) Time pulse waveform after multi-pass amplification and (b) the value of the square pulse distortion for each pass.

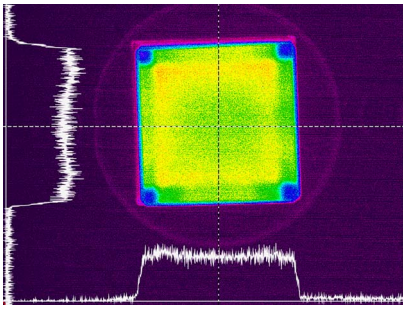

Fig. 6. Fluorescence distribution of Nd:glass amplifier.

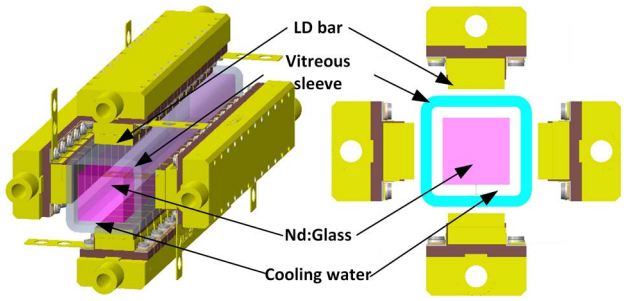

Fig. 5. Nd:glass square rod amplifier structure.

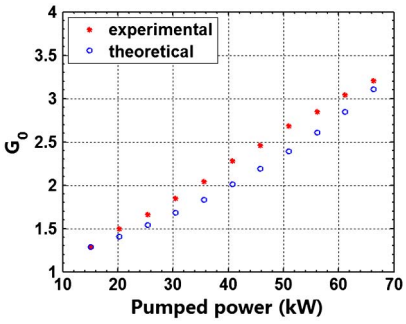

Fig. 7. Influence of pump power on Nd:glass amplifier gain.

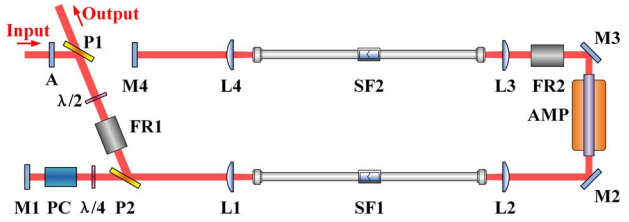

Fig. 8. Four-pass amplification light path diagram. AMP: amplifier; FR: Faraday rotator; L: len; M: mirror; P: polarizer; PC: pockels cell; SF: spatial filter.

coaxial four-pass amplification structure that meets the image-relaying relation is designed as shown in Fig. 8. From diaphragm A, the light beam aperture becomes 10 mm × 10 mm. The incident linearly polarized beam is reflected by the polarizer P1; the polarization is unchanged when passing by the Faraday rotator FR1 and $\lambda/2$ wave plate. After being reflected by the polarizer P2, the incident beam comes to the Nd:glass amplifier for the first-pass amplification. The second-pass amplification occurs in the Nd:glass amplifier after the reflector M4. The polarization is 90° after two passes through FR2, and the beam then transmits from polarizer P2. The electro-optic switch is on by $\lambda/4$ voltage working together with the $\lambda/4$ wave plate. The laser polarization remains unchanged out of the total reflective mirror, and the laser beam still transmits from polarizer P2 coming into the Nd:glass amplifier for the third-pass amplification. The 4th-pass amplification occurs after being reflected by the reflector M4. After passing by the Faraday rotator FR2 two times, the beam will be rotated another 90° and gets reflected by polarizer P2. After passing by Faraday rotator FR1 and the $\lambda/2$ wave plate, the laser beam polarization rotates 90° and is transmitted from polarizer P1. During the process of the fourth-pass amplification, the transmission that meets the image relaying provides the best guarantee of the output beam quality. The aperture position is the object position that is imaged on the center of the Nd:glass amplifier after passing through lenses L1 and L2. The center will be taken as the new object position for the next level transmission and will create an image on the reflector M4 with lenses L3 and L4. The spatial filters SF1 and SF2 among the imaging lens group filter out the light beam of high-frequency modulation and restrain the laser beam's small-scale self-focusing.

Under the condition of a 1 Hz repetition frequency, 50 mJ of injected polarized seed-light energy, a 10 mm × 10 mm aperture, and 66.36 kW pump power of the Nd:glass amplifier, the output laser energy testing result out of the four-pass amplification is shown in Fig. 9; it has an output energy stability of 2.94% (RMS). It can be proven that the Nd:glass square rod amplifier is of good energy stability. The laser spectrum experiences little change before and after amplification, as shown in Fig. 10. The pulse waveforms before and after amplification are measured by an Agilent DSO81204A 12G oscilloscope and a Thorlabs 8G high-speed fiber photoelectric detector,

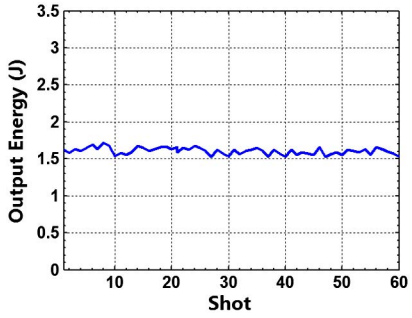

Fig. 9. Energy stability of the Nd:glass amplifier.

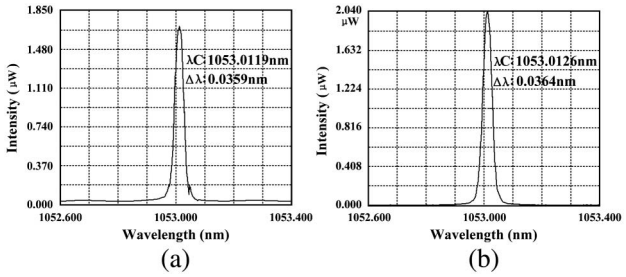

Fig. 10. Spectrum diagram (a) seed and (b) after amplification.

as shown in Fig. 11, from which it can be seen that the square pulse distortion out of the four-pass amplification is less than 2.

In this Letter, a numerical simulation and experimental research are carried out on a laser diode array side-pumped Nd:glass square rod amplifier. The laser-diode side pumping is adopted for amplifying the mid-aperture laser beam energy to realize the repetitive operation. An Nd:glass square rod amplifier of an aperture of 12 mm × 12 mm is developed with the fluorescence evenly distributed. When the pump power is 66.32 kW, the small signal gain increases by 3.23 times. The output energy of the laser beam could reach 1.62 J after the four-pass amplification under the conditions of 1 Hz repetition frequency, 50 mJ of injected seed-light energy, and a 10 mm × 10 mm aperture. The energy amplification of the injected laser beam from millijoules to joules is realized. The output energy stability of the laser pulse is 2.94% (RMS), and the square pulse distortion is smaller than 2. Obviously,

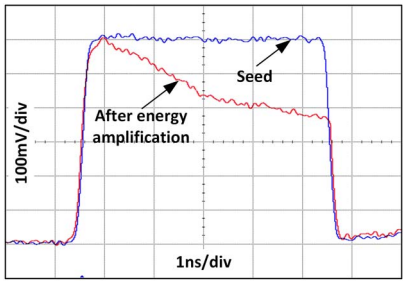

Fig. 11. Time waveform diagram.

the control and optimization of the output laser beam quality will become the focus of the next step.

This work was supported by the National Research and Development Projects for Key Scientific Instruments "Development of high power nanosecond laser and precision detecting instrument."

References

1. B. M. V. Wonterghem, J. R. Murray, J. H. Campbell, D. R. Speck, C. E. Barker, I. C. Smith, D. F. Browning, and W. C. Behrendt, Appl. Opt. **36**, 4932 (1997).
2. J. Lindl, Phys. Plasmas. **2**, 3933 (1995).
3. A. A. Kuzmin, E. A. Khazanov, and A. A. Shaykin, Opt. Express **19**, 14223 (2011).
4. X. Ye, T. Fang, Z. Wang, S. Dai, and J. Xu, Chin. Opt. Lett. **3**, 527 (2005).
5. C. A. Haynam, P. J. Wegner, J. M. Auerbach, M. W. Bowers, S. N. Dixit, G. V. Erbert, G. M. Heestand, M. A. Henesian, M. R. Hermann, K. S. Jancaitis, K. R. Manes, C. D. Marshall, N. C. Mehta, J. Menapace, E. Moses, J. R. Murray, M. C. Nostrand, C. D. Orth, R. Patterson, R. A. Sacks, M. J. Shaw, M. Spaeth, S. B. Sutton, W. H. Williams, C. C. Widmayer, R. K. White, S. T. Yang, and B. M. Van Wonterghem, Appl. Opt. **46**, 3276 (2007).
6. A. K. Sharma, M. Raghuramaiah, K. K. Mishra, P. A. Naik, S. R. Kumbhare, and P. D. Gupta, Opt. Commun. **252**, 369 (2005).
7. Y. Peng, J. Wang, Z. Zhang, D. Huang, W. Fan, and X. Li, Chin. Opt. Lett. **12**, 041402 (2014).
8. A. A. Kuzmin, E. A. Khazanov, and A. A. Shaykin, Opt. Express **19**, 14223 (2011).
9. X. K. Cheng, Q. J. Cui, Y. Zhou, Z. M. Wang, J. L. Xu, Y. Bo, Q. J. Peng, D. F. Cui, and Z. Y. Xua, Opt. Commun. **281**, 4288 (2009).
10. F. Friebel, A. Pellegrina, D. N. Papadopoulos, P. Camy, J. Doualan, R. Moncorgé, P. Georges, and F. Druon, Appl. Phys. B **117**, 597 (2014).
11. A. Berrou, T. Lbach, and M. Eichhom, Appl. Phys. B **120**, 105 (2015).
12. Q. H. Deng, H. S. Peng, S. X. Gao, M. Z. Li, L. Ding, J. Lei, J. J. Wang, Y. M. Luo, J. Tang, H. H. Lin, R. Zhang, Y. Deng, and Z. H. Lu, Chin. J. Lasers **36**, 70 (2009).
13. T. T. Zhao, J. Yu, L. Q. Hou, Y. F. Ma, Y. Liu, X. Zhang, Y. Yan, and Z. W. Fan, Opt. Laser Technol. **44**, 26 (2012).
14. A. Bayramian, P. Armstrong, E. Ault, R. Beach, C. Bibeau, J. Caird, R. Campbell, B. Chai, J. Dawson, C. Ebbers, A. Erlandson, Y. Fei, B. Freitas, R. Kent, Z. Liao, T. Ladran, J. Menapace, B. Molander, S. Payne, N. Peterson, M. Randles, K. Schaffers, S. Sutton, J. Tassano, S. Telford, and E. Utterback, Fusion Sci. Technol. **52**, 383 (2007).
15. M. Bowers, S. Burkhart, S. Cohen, G. Erbert, J. Heebner, M. Hermann, and D. Jedlovec, Proc. SPIE **6451**, 64511M (2007).
16. J. C. Chanteloup, H. Yu, G. Bourdet, C. Dambrine, S. Ferre, A. Fulop, S. Le Moal, A. Pichot, G. L. Touze, and Z. Zhao, Proc. SPIE **5707**, 105 (2005).
17. W. Koechner, *Solid-State Laser Engineering* (Springer-Verlag, 2006).
18. S. G. Li, S. B. Chen, L. Wen, L. L. Hu, and B. Wang, High Power Laser Part. Beams **15**, 1159 (2003).
19. Z. G. Jiang and Z. M. Yang, Chin. J. Lasers **37**, 2198 (2010).